Dynamics of Atmospheres and Oceans 47 (2009) 15–37

Contents lists available at ScienceDirect

Dynamics of Atmospheres and Oceans

journal homepage: www.elsevier.com/locate/dynatmoce

Review

Multi-scale climate variability of the South China Sea monsoon: A review

Bin Wang[a,*], Fei Huang[b], Zhiwei Wu[c], Jing Yang[d], Xiouhua Fu[a], Kazuyoshi Kikuchi[a]

[a] *Department of Meteorology and International Pacific Research Center, School of Ocean and Earth Science and Technology, University of Hawaii, Honolulu, HI 96822, USA*
[b] *Ocean-Atmosphere Interaction Laboratory (OAC), Department of Marine Meteorology, Ocean University of China, Qingdao 266100, China*
[c] *LASG, Institute of Atmospheric Physics, Chinese Academy of Sciences, Beijing 100029, China*
[d] *State Key Laboratory of Earth Surface Processes and Resource Ecology, Beijing Normal University, Beijing 100875, China*

ARTICLE INFO

Article history:
Available online 17 October 2008

Keywords:
South China Sea
Monsoon

ABSTRACT

This review recapitulates climate variations of the South China Sea (SCS) monsoon and our current understanding of the important physical processes responsible for the SCS summer monsoon's intraseasonal to interannual variations. We demonstrate that the 850 hPa meridional shear vorticity index (SCSMI) can conveniently measure and monitor SCS monsoon variations on a timescale ranging from intraseasonal to interdecadal. Analyses with this multi-scale index reveal that the two principal modes of intraseasonal variation, the quasi-biweekly and 30–60-day modes, have different source regions and lifecycles, and both may be potentially predicted at a lead time longer than one-half of their corresponding lifecycles. The leading mode of interannual variation is seasonally dependent: the seasonal precipitation anomaly suddenly reverses the sign from summer to fall, and the reversed anomaly then persists through the next summer. Since the late 1970s, the relationship between the SCS summer monsoon and El Niño-Southern Oscillation (ENSO) has significantly strengthened. Before the late 1970s, the SCS summer monsoon was primarily influenced by ENSO development, while after the late 1970s, it has been affected mainly in the decaying phase of ENSO. The year of 1993 marked a sudden interdecadal change in precipitation and circulation in the SCS and

* Corresponding author. Tel.: +1 808 956 2563; fax: +1 808 956 9425.
E-mail address: wangbin@hawaii.edu (B. Wang).

0377-0265/$ – see front matter
doi:10.1016/j.dynatmoce.2008.09.004

its surrounding region. Over the past 60 years, the SCS summer monsoon's strength shows no significant trend, but the SCS winter monsoon displays a significant strengthening tendency (mainly in its easterly component and its total wind speed). A number of outstanding issues are raised for future studies.

Contents

1. Introduction

The South China Sea (SCS) is a marginal sea located in Southeast Asia roughly between the equator and 22°N and from 110°E to 120°E (Fig. 1). Geographically, the SCS resides at the center of the Asian-Australian monsoon (30°S–40°N, 40°E–170°E) and joins four monsoon subsystems: the subtropical East Asian (EA) monsoon, the tropical Indian monsoon, the western North Pacific (WNP) monsoon, and the Australian monsoon. Fig. 1 presents the differential precipitation pattern between June/July/August (JJA) and December/January/February (DJF); this underlines the differential latent heating between the Northern Hemisphere (NH) and Southern Hemisphere (SH), which drives the annual cycle of the Asian-Australian monsoon.

While the SCS summer monsoon (SCSSM) has been regarded as a part of the EA summer monsoon (EASM; e.g., Zhu et al., 1986; Tao and Chen, 1987; Ding, 1992), it is a typical tropical monsoon and is more closely linked to the tropical WNP monsoon (Murakami and Matsumoto, 1994; Wang, 1994). Because of its special geographic location and unique monsoon characteristics, which will be discussed shortly, the SCS monsoon has been one of the foci of monsoon research, especially after the SCS Monsoon Experiment (SCSMEX) in 1998 (Lau, 1995; Lau et al., 2000; Ding et al., 2004).

Of great scientific importance is the prominent climate variability of the SCS monsoon on intraseasonal to geological timescales. On the intraseasonal timescale, the SCS exhibits the largest intraseasonal (10–100-day) variability in the Asia-Pacific region during boreal summer (Kemball-Cook and Wang, 2001). The westward-propagating quasi-biweekly (QBW) mode originating from the SCS and the Philippines have significant influences on Indochina, the Bay of Bengal, and India (Chen and Chen, 1993). The northward-propagating 30–50-day mode from the SCS seems to be linked to the occurrence of extreme rainfall events in subtropical East Asia (Zhu et al., 2003). During northern summer, convective bursts over the northern SCS and the Philippines extend their influences all the way to North America through the establishment of a circum-Pacific Rossby wave

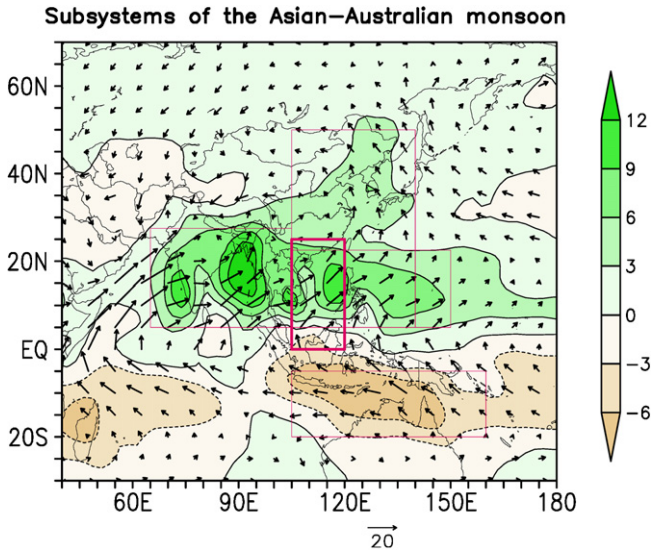

Fig. 1. Climatological mean June/July/August (JJA) minus December/January/February (DJF) precipitation rates (color shading in mm/day) and 925 hPa wind vectors (arrows) in Asian-Australian monsoon region. The precipitation climatology is derived from CMAP (Xie and Arkin, 1997) (1979–2006) and wind climatology from NCEP/DOE reanalysis (1979–2006) (Kanamitsu et al., 2002). The four boxes define major summer precipitation areas of the Indian monsoon (5°N–27.5°N, 65°E–105°E), western North Pacific monsoon (5°N–22.5°N, 105°E–150°E), East Asian subtropical monsoon, and Australian monsoon. The South China Sea monsoon is indicated by the thick solid rectangular.

train (Kawamura et al., 1996; Fukutomi and Yasunari, 2002). On the annual timescale, the onset of the SCS summer monsoon (SCSSM) signifies the onset of the large-scale summer monsoon over EA and the WNP (Tao and Chen, 1987). The SCS also acts as a water vapor pathway connecting the Indian and EA-WNP monsoon during boreal summer and connecting the most powerful EA winter monsoon with the Australian summer monsoon (Fig. 1). During boreal winter, the SCS encounters the strongest tropical–extratropical interaction, hemispheric interaction, and multi-scale interaction. The year-to-year variability of SCSSM precipitation acts as an anomalous heat source, further influencing EA, India, and Australia (e.g., Tao and Chen, 1987; Ding, 1992; Lau and Yang, 1997; Wang et al., 2004). On the orbital and geological timescales, sediment recorded in SCS monsoon upwelling regions provides valuable information about the variability of the EASM (Wang, 1999).

Understanding of the SCS monsoon's climate variability is a great challenge because the sources of variability are complicated due to influences from the four adjacent monsoon subsystems. The equatorial Madden and Julian (1971, 1972, 1994) Oscillation (MJO) has a significant influence on the SCS. Cold surges and baroclinic waves from the north or west and tropical storms and disturbances from the east also propagate into the SCS and cause synoptic and intraseasonal fluctuations. As such, the summer monsoon onset and winter monsoon multi-scale interaction have attracted extensive attention in previous studies (Chang et al., 2006). The SCS is also a region of tropical cyclogenesis, hosting most typhoons or tropical storms that pass through the Philippines and make landfall in southern China and Vietnam. The tropical cyclone (TC) activity is significantly modulated by intraseasonal to interdecadal climate variations.

The principal goal of this review is to provide a concise synopsis of the distinct multi-scale climate variability of the SCS monsoon and to discuss the physical processes that give rise to this variability. We first review unique features of the seasonal march in Section 2. For dynamic consistency, we propose a unified multi-scale circulation index to describe the climate variability on timescales ranging from intraseasonal to interdecadal (Section 3). An account is then given to intraseasonal variations (Section 4), interannual variations (Section 5), interdecadal variability (Section 6), and the long-term trend

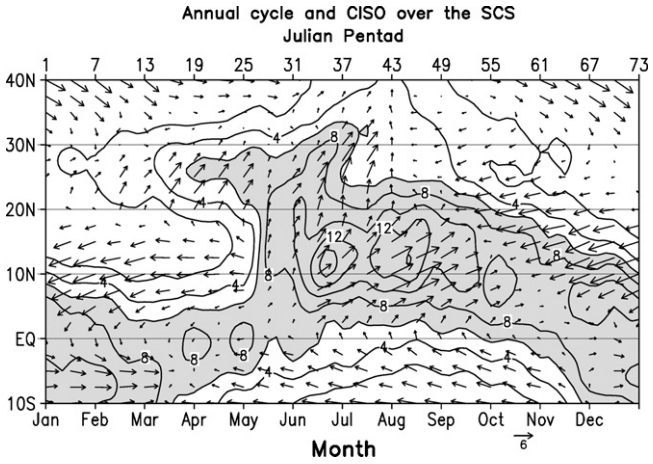

Fig. 2. Climatological pentad mean 850 hPa horizontal winds (vector in m/s) and CMAP pentad mean rainfall (contours in units of 2 mm/day) as function of latitude and calendar month. The data are averaged over the longitude bands between 110°E and 120°E across the SCS. The climatology was made using data from 1979 to 2006. The shading denotes precipitation rate exceeding 6 mm/day.

over the past 60 years with instrumental data (Section 7). The last section discusses challenges in understanding numerical modeling and climate prediction of the SCS monsoon.

2. Seasonal march

One of the unique and spectacular features of the SCS monsoon is its abrupt climatological onset occurring in mid-May around Julian Pentad 28 (Fig. 2). The abrupt burst of monsoon rains takes place across a large latitudinal range from 5°N to 22°N with a complete reversal of lower tropospheric zonal wind (from easterly to westerly) between the equator and 18°N. Although the transition from the Asian winter to summer monsoon is in general discontinuous (Meehl, 1987; Yasunari, 1991; Matsumoto and Murakami, 2002; Hung and Yanai, 2004), the remarkable abruptness in the establishment of the summer southwesterly and the burst of monsoon rains distinguishes the SCSSM from any of other regional monsoons.

Following the SCSSM onset is a swift expansion of the onset region from SCS all the way to 160°E in the subtropical Pacific (Wang and LinHo, 2002). This extension of climatological onset takes only 5 days or so, which signifies a full establishment of the EA subtropical frontal rain band. For this reason, the SCSSM onset is regarded as a precursor of the EASM onset (Tao and Chen, 1987; Tanaka, 1992). Note also that the northward migration of the subtropical rain band from 20°N to 40°N after the SCSSM onset is the most spectacular seasonal march of the rain band on Earth.

In contrast to the abrupt onset, the mean monsoon retreat in the SCS is gradual, taking about 3 months (from September to November) to reverse wind direction from southwesterly to northeasterly across its full latitudinal extent (Fig. 2). This equinoctial (spring–autumn) asymmetry in seasonal transition is notable, reflecting a large-scale feature over the entire Asian-Pacific monsoon system: the early start of the rainy season over the Southeast Asian continent in boreal spring, and the late retreat over the SCS and WNP in boreal autumn (Chang et al., 2005a; Wang and Ding, 2008).

The seasonal march of the SCS monsoon has a prominent component called climatological intraseasonal oscillation (CISO; Nakazawa, 1992; Wang and Xu, 1997; Kang et al., 1999) or the "fast" annual cycle (LinHo and Wang, 2002). CISO is the portion of ISO that is phase-locked to the annual cycle (Wang and Xu, 1997). CISO signals can be readily recognized from Fig. 2. Three notable increases in precipitation and corresponding surges of southwesterly occur, around Pentad 28 (May 16–20), Pentad 34–35 (June 15–24), and Pentad 46–47 (August 14–23); see Fig. 2. The three wet phases of CISO cycles signify the SCSSM onset, peak Maiyu/Baiu, and peak WNP summer monsoon, respectively (Wang and Xu,

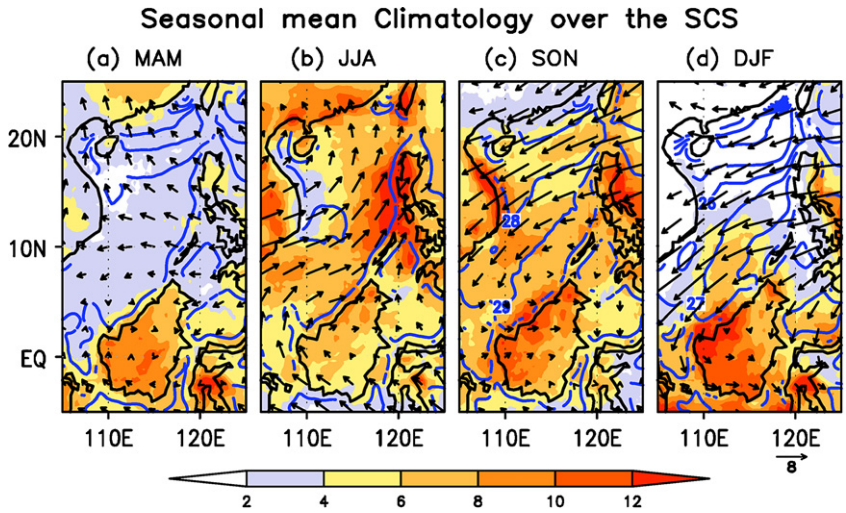

Fig. 3. Climatological seasonal mean precipitation rates (color shading in mm/day), 925 hPa wind vectors (arrows in m/s), and SST (contours in °C) in the SCS region (5°S–25°N, 105°E–125°E) for (a) MAM, (b) JJA, (c) SON, (d) DJF. The climatology is based on 10 years for 1998–2007. The precipitation is derived from Tropical Rainfall Measuring Mission (TRMM) 3B42 version 6 product, the winds from NCEP/DOE AMIP-II Reanalysis (Kanamitsu et al., 2002), and SST from TRMM Microwave Imager (TMI).

1997). Around Pentad 46–47, the precipitation increase is not as significant as in the first two CISO wet phases, but the southwesterly monsoon surge is more significant. This is because the third CISO wet phase represents a Rossby wave response to the sudden precipitation change over the Philippine Sea. As such, the southwesterly monsoon surge over the SCS is more significant than its rainfall variation. CISO tends to propagate northward. Most prominent is the northward propagation of the CISO wet phase that is associated with the SCSSM onset, which reflects seasonal march of the subtropical rain band from late May to late July and from 20°N to 40°N. The stepwise migration (Ding, 1992) can be most evidently seen from the CISO component, not the total rainfall (Liu et al., 2008).

The northeasterly winds during boreal winter are strongest on the same latitude circle. As a result, the high SST region associated with the Indo-Pacific warm pool is split along the western SCS due to enormous cooling induced by cold advection, evaporation, and entrainment (Liu et al., 2004). Note also that the maximum precipitation zone (or intertropical convergence zone, or "ITCZ") during November and December remains in the southern SCS, signifying an active winter monsoon rainy season there (Fig. 2). Due to interaction between northeast monsoon and the terrain on Borneo Island, vortices near the northwestern coast of Borneo have a higher frequency of occurrence than any of the other quasi-stationary synoptic disturbances in the entire equatorial belt (Chang et al., 2005a). During early winter, the southern SCS is a region where the QBW's cold surges from the north, the 30–60-day MJO (Madden and Julian, 1971, 1972) from the west, and the synoptic-scale Boneo vortices all actively interact with each other (Chang et al., 2005a,b). The ITCZ becomes its weakest and the SCS is its driest during the pre-monsoon period from March to mid-May (Fig. 2). Nearly the entire SCS is controlled by an elongated subtropical ridge, and SST in the entire SCS increases steadily to reach its annual maximum before the monsoon's onset.

Although the longitudinal span of the SCS is only about 10° of longitude, the summer monsoon rainfall has a pronounced east–west contrast over the central SCS (Fig. 3b). The precipitation in the west (110°E) is only about one quarter of that in the east (120°E). This sharp contrast in east–west precipitation arises from significant east–west SST gradients: cold around the Vietnam coast and warm to the west of the northern Philippines (Wang and Wu, 1997). The former is caused by upwelling induced by the along-shore southwest monsoon, while the latter is due to deepening thermocline as a result of Upper Ocean Ekman transport driven by the southwest monsoon (Liu et al., 2000).

The seasonal distribution of precipitation also has considerable latitudinal variations (Fig. 3). While the rainy season in the northern and eastern central SCS peaks in August, the southern SCS (south of 8°N) exhibits a prominent semi-annual cycle with a major peak in November–December (winter monsoon) and a minor peak in June (summer monsoon). In the western central SCS, a similar semiannual cycle exists with a double rainfall peak corresponding to the onset and withdrawal of the summer monsoon, resembling Indochina's rainy season characteristics. Note also that the monsoon–topography interaction in the surrounding region of the SCS is prominent. A large amount of rainfall occurs along the east coasts of the Philippines, Vietnam, and the Malaysian peninsula during winter.

In summary, the seasonal march of the SCS monsoon exhibits a number of unique features: the abrupt simultaneous onset over a 20° latitude range; the rapid northeastward "expansion" of the onset that establishes the EA summer subtropical front; the conspicuous spring–autumn asymmetry in seasonal transition; the pronounced CISO and monsoon singularities; the strongest winter monsoon in the tropics; the most active tropical–extratropical interaction, hemispheric interaction, and multiscale interaction; and the prominent east–west gradient of precipitation. These atmospheric features impact forced monsoon ocean circulation and SST as well as atmosphere-ocean interaction, making the SCS monsoon oceanography interesting for study (see other reviews in this special issue).

3. A multi-timescale South China Sea monsoon index

One of the major roadblocks in the current study of SCS climate variability is the lack of a generally recognized measure of summer monsoon intensity, especially on the interannual and interdecadal timescales. In this section, we explore the possibility of defining a simple, objective circulation index that can apply to a variety of timescales. Ideally, precipitation is the best measure because it depicts heat source-driving monsoon circulation and is the most important variable, practically speaking. But SCS precipitation estimated by rain gauges is sparse, and SCS precipitation records estimated by satellites are limited in length. Thus, for the study of interdecadal variability, a circulation index is desirable. So then, the issue is, how to construct an objective circulation index that can depict both the precipitation and circulation variability over the SCS?

The precipitation over the SCS can be well represented by its mean value averaged over the central-northern SCS (7°N–20°N, 110°E–120°E). When the precipitation in this core region is enhanced, what are the characteristics of the associated circulation anomalies? Are the circulation anomalies dependent on timescales? Fig. 4 compares the precipitation–850 hPa circulation relationship on the broad sebseasonal (Fig. 4a and b) and interannual timescales (Fig. 4c and d).

Fig. 4a shows that on an intraseasonal timescale, the enhanced precipitation corresponds to an enhanced cyclonic circulation anomaly at 850 hPa. The cyclonic center (16°N, 115°E) is located slightly to the north of the precipitation center at (13.5°N, 115°E). Note that the westerly anomalies to the south of the cyclonic center cover a much larger region than the easterly anomalies to the north of the cyclone center (Fig. 4a). This pattern can be understood as a Rossby wave response to a given heating implied by the SCS precipitation (Gill, 1980).

The circulation anomalies associated with the enhanced SCS precipitation (shown in Fig. 4a) may be concisely described by the following meridional shear vorticity index (for simplicity, SCSMI hereafter):

$$\mathrm{SCSMI} = \mathrm{U850}(5^\circ\mathrm{N}\text{–}15^\circ\mathrm{N},\ 110^\circ\mathrm{E}\text{–}120^\circ\mathrm{E})\ \ \mathrm{minus}\ \ \mathrm{U850}(20^\circ\mathrm{N}\text{–}25^\circ\mathrm{N},\ 110^\circ\mathrm{E}\text{–}120^\circ\mathrm{E}),$$

where the first and second terms on the right-hand side represent 850 hPa zonal wind averaged over (5°N–15°N, 110°E–120°E) and over (20°N–25°N, 110°E–120°E), respectively.

On an intraseasonal timescale, a positive (negative) vorticity index represents active (break) phase of the SCS's summer monsoon, during which convection is enhanced (suppressed). Fig. 4b indicates that when the northern SCS is in a wet phase, the Maritime Continent to its south and southern China to its north are in a dry phase.

Can the afore-defined SCSMI be used to characterize interannual variation? Fig. 4c shows that on the interannual timescale, enhanced JJA precipitation in the SCS corresponds to an enhanced cyclonic circulation anomaly at 850 hPa and enhanced westerlies from the Bay of Bengal to the Philippine Sea, a

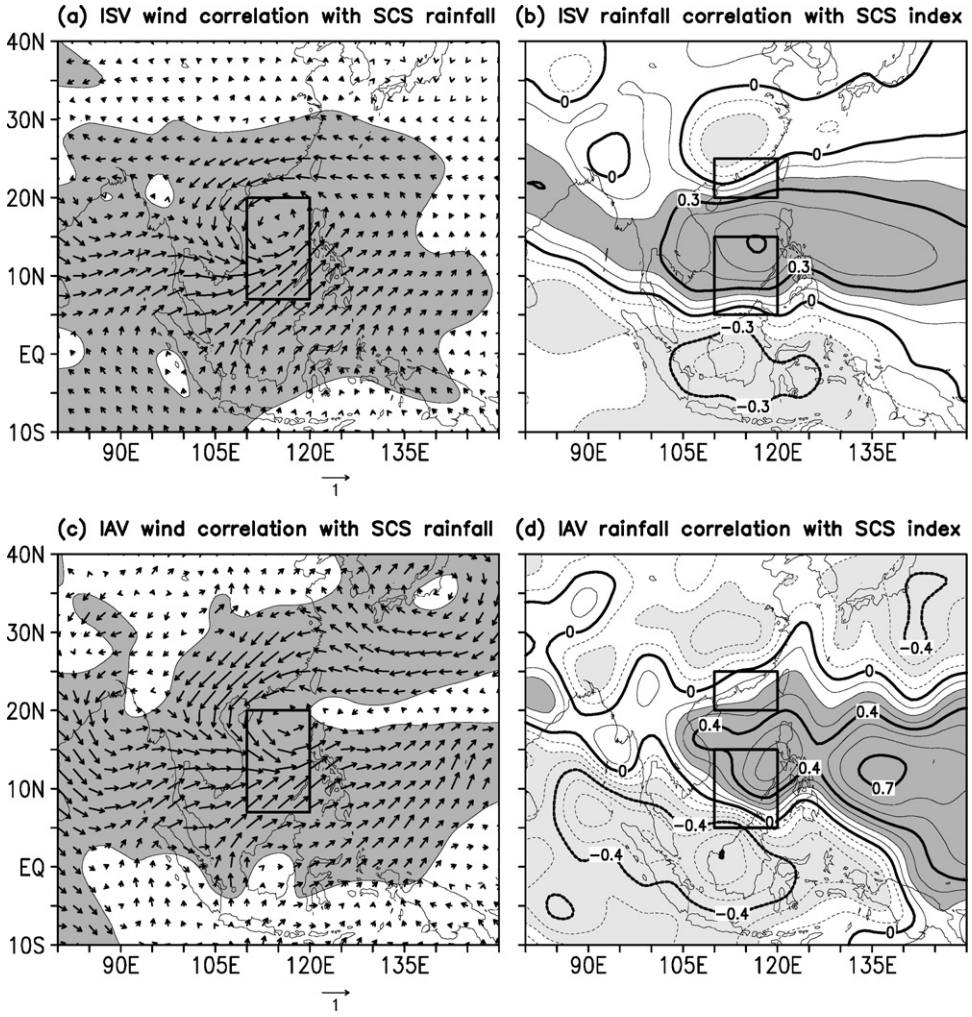

Fig. 4. (a) Vector correlation map of the pentad mean 850 hPa winds with reference to the pentad mean precipitation rate averaged over the central-northern SCS (the thick black rectangular box: 7°N–20°N, 110°E–120°E). The zonal and meridional components of the vectors represent, respectively, the correlation coefficients of the zonal and meridional winds with the precipitation. The positive rainfall anomaly corresponds to the eastward and northward wind anomalies, respectively. The light shadings indicate statistical significance exceeding 99% confidence level. (b) Correlation map of the pentad CMAP rainfall rate with reference to the SCS monsoon index (SCSMI): the 850 hPa zonal wind averaged over (5°N–15°N, 110°E–120°E) minus that averaged over (20°N–25°N, 110°E–120°E). The two blue rectangular regions indicate the regions selected for defining the SCSMI. The data used for calculation of correlation coefficients are from pentad 25 (May 1–5) to pentad 55 (September 28–October 2) for the period of 1979–2006. (c) and (d) are the same as in (a) and (b) except for the JJA mean anomalies from 1979 to 2006.

pattern similar to that seen on an intraseasonal timescale. This similarity arises from the same process of Rossby wave response to precipitation heating. However, notable circulation differences between the two timescales are seen in the Philippine Sea and subtropical-mid-latitude EA. On the interannual timescale, the cyclonic anomaly is located to the north of the SCS precipitation center and extends eastward along 20°N, which implies a weakening of the normal WNP subtropical ridge along 20°N. In addition, there is a strong anticyclonic anomaly centered on southeast Japan. For the same precipitation anomaly in the central-north SCS, why does the corresponding circulation on the interannual timescale differ from the intraseasonal timescale? We argue that the differences arise from the effects of the

monsoonal mean flows. The year-to-year fluctuation is modulated by the climatological mean state (Fig. 1 and Fig. 3b). The anomalous precipitation heating would disturb both the WNP monsoon trough and subtropical high; as such, the cyclonic anomalies extend eastward and have an elongated shape. The eastward extension of the Philippine Sea anomaly affects the circulation anomaly over Japan through Pacific-Japan teleconnection (Nitta, 1987). On the other hand, the pentad mean circulation anomalies represent averaged response across the May–October season, during which the basic state experiences large changes but its effects minimized due to cancellation.

On the interannual timescale, a positive value of the SCS vorticity index represents abundant rainfall, and thus a strong SCS monsoon (Fig. 4d). When SCS summer monsoon is strong, the WNP monsoon over the Philippine Sea is also intensified. This in-phase variability is a robust feature, as shown by the large positive correlation coefficient (Fig. 4d). A strong SCSSM is also accompanied by deficient precipitation over the Maritime Continent and southeast Bay of Bengal and along the Meiyu/Baiu front extending from the Yangtze River Valley and southern Japan. There exists a seesaw relationship in rainfall between the SCS and subtropical East Asia. Wang et al. (2008a) showed that the leading mode of the entire EA-WNP SM system can be very well measured by the Wang–Fan (Wang and Fan, 1999) index. Although the SCS vorticity index is designed as a local measure of the strength of the SCSSM, the correlation coefficient between the SCS vorticity index and large-scale Wang–Fan index is 0.94 for the period of 1948–2007, suggesting that this SCS index has large-scale implications.

In summary, the proposed SCS meridional shear vorticity index can represent both the active-break cycles of the intraseasonal variability and the interannual variability over the SCS and adjacent regions. While we focus on boreal summer variability in this section, this index can represent the annual cycle and intraseasonal to interdecadal variations throughout the annual cycle. In the next three sections, we will demonstrate its applicability in depicting the SCS monsoon's multi-timescale variability.

4. Intraseasonal variations

During northern summer from May to October, intraseasonal variation (ISV) over the SCS is concentrated on two frequency bands: 12–25 days and 30–60 days (e.g., Chen and Chen, 1995; Fukutomi and Yasunari, 1999; Annamalai and Slingo, 2001; Chan et al., 2002). A spectral analysis of the daily SCS meridional shear vorticity index confirms that the vorticity variability indeed has two major peaks: one on the QBW (12–25 days) timescale and the other on the 30–50-day timescale (figure not shown). The magnitude of the QBW variance over the SCS is comparable to the corresponding 30–50-day variance (especially between 10°N and 20°N). Here we use the SCSMI as a reference to describe behaviors of the two ISV modes, with emphasis on their different lifecycles and discussion of the mechanisms of ISV.

4.1. Contrasting lifecycles of the 30–50-day and QBW oscillations

The propagation of the 30–50-day oscillation during boreal summer involves complex patterns. Previous studies have identified a number of pathways, including (1) northward propagation connected with the eastward-propagating MJO (Chen and Murakami, 1988; Wang and Rui, 1990; Lawrence and Webster, 2002), (2) northwestward propagation from the equatorial western Pacific (Lau and Chan, 1986; Nitta, 1987), (3) merging of an equatorial eastward-moving convective system and a westward-propagating lower-level convergence anomaly located in the subtropics (Hsu and Weng, 2001), and (4) independent northward propagation (Wang and Rui, 1990).

Fig. 5a shows the propagation of an outgoing longwave radiation (OLR) anomaly during a lifecycle of the 30–50-day oscillation regressed with reference to the SCSMI derived from 29 summers (May–October) for 1979–2007. Enhanced precipitation first emerges in the central equatorial Indian Ocean (Day −11) and then moves eastward and develops along the equator (Day −5). In the second phase, the precipitation anomaly moves into the Maritime Continent; meanwhile, it bifurcates poleward (Day 0) and then forms a major rain band tilted in the northwest–southeast direction over the northern Indian Ocean (Day 5). In the third phase, the NW–SE tilted rain band moves northeastward, and the equatorial portion moves from the Maritime Continent into the equatorial western Pacific (Day +11). This completes a half cycle. The next half cycle is a mirror image of the first half cycle (but the

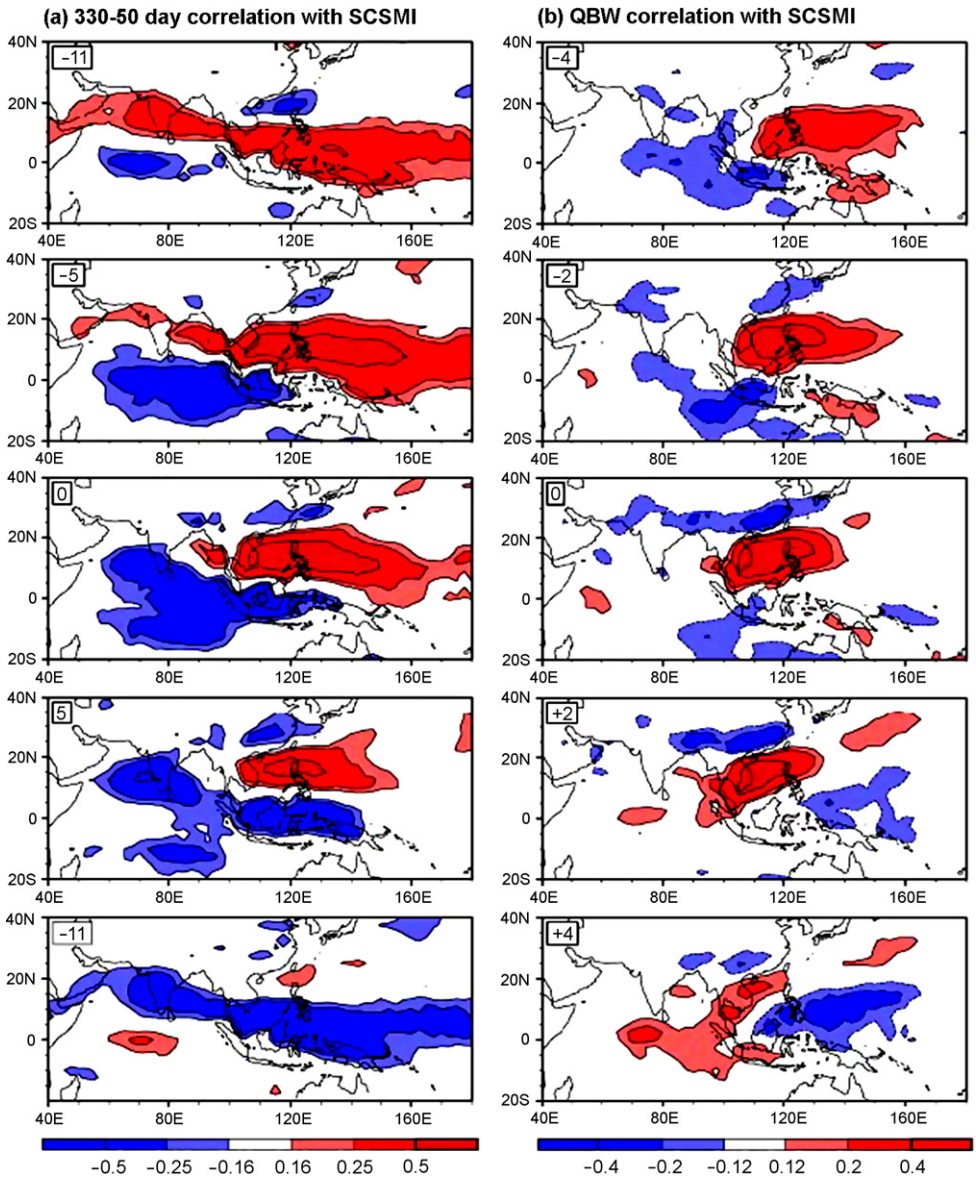

Fig. 5. (a) Life cycle of the 30–50-day oscillation mode, which is shown by the lead-lag correlation coefficients between the OLR field and the SCSMI from −11 days to +11 days with the 0-day denoting the maximum dry phase at the SCS. Shadings indicate statistical significance exceeding 95% confidence level. The calculations are based on 29 boreal summers (May–October) from 1979 to 2007. (b) The same as in (a) but for the quasi-biweekly (12–25 days) mode from −4 days to +4 days.

actual dates should be understood as the dates shown in each panel plus 22 days). The fourth stage from Day 11 to 17 (or Day −11 to Day −5 with opposite signs) features a northwestward migration from the equatorial western Pacific toward SCS, finally reaching the SCS at Day +27 (Day +5 with opposite sign).

The overall propagation features shown in Fig. 5a are consistent with previous findings regarding boreal summer intraseasonal oscillation that were obtained using different methods, such as empirical

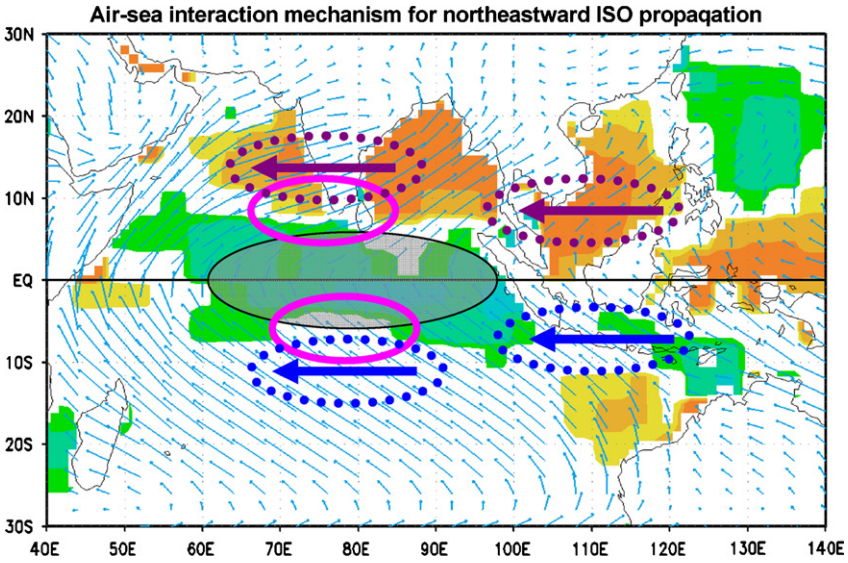

Fig. 6. Schematic diagram illustrating the mechanism by which air–sea coupling sustains northeastward propagation of the boreal summer intraseasonal oscillation. This figure highlights the mechanism proposed by Fu et al. (2003) and Fu and Wang (2004). Background arrows denote seasonal mean 925 hPa winds. Color shading indicates SST anomalies associated with BSISO, Shaded elliptic circle denotes convective anomaly, and heavy arrows denote anomalous BSISO winds. Detailed explanation refers to the text.

orthogonal function (EOF) analysis (Lau and Chan, 1986; Ferranti et al., 1997), principal pattern oscillation analysis by Annamalai and Slingo (2001), composite analysis (Kemball-Cook and Wang, 2001; Wang et al., 2006), and extended EOF analysis (Waliser et al., 2006). Note that Fig. 6a is derived with reference to the SCS vorticity index, but the obtained lifecycle is in excellent agreement with previous results that stress the equatorial oscillations, suggesting that the propagation pattern and lifecycle of the boreal summer's 30–50-day oscillation is very robust.

The 30–50-day wet anomaly occurring over the equatorial western Pacific tends to lead the wet anomaly over the SCS by about 12 days (Fig. 5a). Similarly, the wet anomalies in the equatorial central Indian Ocean tend to lead the wet phase over the SCS by about 27 days. These lead-correlations provide precursors for the prediction of the SCS 30–50-day oscillation and the active-break phase of the SCS summer monsoon.

The QBW oscillation was first found in the Indian summer monsoon (Krishnamurti and Bhalme, 1976; Murakami, 1976), and later in EA, the SCS, Indo-China, and the WNP (Murakami, 1980; Lau and Chang, 1992; Tanaka, 1992; Chen and Chen, 1993; Chen and Yoon, 2000). The QBW oscillation in the SCS is more active than in the Indian summer monsoon region.

Fig. 5b shows a half-life cycle and propagation route of the QBW convective anomaly (negative OLR) that affects the SCS. The QBW anomaly has different propagation from that of the 30–50-day oscillation. When the Philippine Sea is in a dry phase (Day −4), active convection is located in the equatorial eastern Indian Ocean and Sumatra. On Day 0, the dry anomaly moves westward to the SCS at the same time that South China becomes wet. From Day 0 to Day +4, there is a tendency toward southwest extension of the dry anomaly from the SCS to the equatorial eastern Indian Ocean, while a new wet anomaly emerges over the western Pacific (Day +2) and then moves to the southern Philippine Sea (Day +4). Thereafter, the wet anomaly evolves in the same way as the dry anomaly described above. The precise reason for the emergence of a wet (or dry) anomaly over the western Pacific is not clear. But the northward and westward propagation from the equatorial western Pacific to the SCS is robust. This correlated pattern derived from the 29-year summer data agrees well with the northwest propagation over the WNP depicted in the previous studies (Krishnamurti and Ardanuy, 1980; Murakami, 1980; Chen and Chen, 1995; Fukutomi and Yasunari, 1999; Annamalai and Slingo, 2001; Mao and Chan,

2005). The off-equatorial westward-propagating QBW mode is perceived as a moist equatorial Rossby wave modified by the basic state (Wang and Xie, 1997; Chatterjee and Goswami, 2004) or a mixed Rossby-Gravity wave (e.g., Goswami and Mathew, 1994; Mao and Chan, 2005).

4.2. Mechanisms of the SCS intraseasonal variations

Northward propagation from the Maritime Continent and the equatorial western Pacific to the SCS is a common and essential feature for both QBW and 30–50-day oscillations. This northward propagation is also a feature that distinguishes these oscillations from the Madden–Julian Oscillation.

What physical processes are responsible for the northward propagation? Two types of processes have been recognized: atmospheric internal dynamics and air–sea interaction. The internal dynamics include easterly vertical shears of the mean flow and boundary layer moisture advection (Jiang et al., 2004; Drbohlav and Wang, 2005). As explained by Wang (2005), the mean-flow easterly vertical shear provides an available equatorward vorticity. The perturbation upward motion associated with ISO decreases northward from the ISO center, which can twist the mean equatorward vorticity, generating cyclonic vorticity to the north of the convective anomaly. The cyclonic vorticity in turn induces convergence in the boundary layer, which destabilizes the atmosphere and triggers new convection to the north of the existing convection. This atmospheric internal mechanism favors northward propagation of ISO.

The air–sea coupled structure for boreal summer ISV was documented in detail by Kemball-Cook and Wang (2001). In general, a positive SST anomaly tends to lead the corresponding precipitation anomaly by about a quarter of a cycle in both a propagating ISO and a stationary ISO. Two types of air–sea interaction theories have been proposed to explain how the air–sea interaction can enhance the ISV and contribute to its propagation. The first is a propagating air–sea interaction theory that explains why a 30–50-day mode propagates northeastward during boreal summer (Fu et al., 2003; Fu and Wang, 2004). Fig. 6 illustrates this mechanism. During boreal summer, the mean low-level southwesterly monsoon prevails in the northern hemisphere tropics, and southeasterly trades prevail in the southern tropics. When ISV-related convection moves to the central-eastern equatorial Indian Ocean, the heating-induced Kelvin wave generates an easterly anomaly to the east of the convection, which intensifies the easterlies in the southern Indian Ocean but reduces the westerlies in the SCS-Bay of Bengal (Fig. 6). Thus, the upward latent heat flux increases in the southern tropics but decreases in the northern tropics, which favors the development of positive (negative) SST anomalies to the north (south) of the equator. Similar processes occur in association with the Rossby wave response to convective heating. The northern (southern) Rossby-like vortex reduces (enhances) surface winds in the northern (southern) side of convection (Fig. 6). The associated changes of latent heat flux tend to warm up (cool down) the northern (southern) tropics. Thus, the anti-symmetric mean zonal flow generates an equatorial asymmetric latent heat flux field. The ISO-related solar radiation change is also important. The reduced downward solar radiation beneath the convection tends to lower SST in the central-eastern equatorial Indian Ocean. Because the summer-mean cloud amount is much larger to the north of 10°S than to south of it, the descending motion associated with convection significantly reduces (increases) the cloud amount (downward solar radiation) in the northern and eastern sides of the convection. Therefore, both the increased downward solar radiation and the reduced evaporation contribute to significant warming in the northern Indian Ocean and the SCS (Fig. 6). The fact that the oceanic mixed layer is shallower in the northern Indian Ocean and deeper in the southern Indian Ocean further enhances the asymmetric SST distribution. The warming to the northeast of the equatorial convective anomaly favors destabilization of the atmospheric boundary layer and increases the convective instability, thus driving the equatorial convective anomaly moving northeastward.

The second mechanism is a stationary air–sea interaction theory (Wang and Zhang, 2002), which is particularly relevant to explain why the ISO in the SCS and the WNP is particularly strong. As shown in the upper panel of Fig. 7, the background flows are controlled by the summer monsoon trough over the northern SCS and the Philippine Sea. When a high-pressure (thus dry) anomaly of ISO moves into the monsoon trough region, total wind speed and thus latent heat loss reduces ($Q_l > 0$) and short wave radiation heating increases ($Q_r > 0$) in the oceanic mixed layer, causing SST to rise (lower panel of Fig. 7) and pressure to decrease. When the anomalous anticyclone disappears, SST anomalies reach a

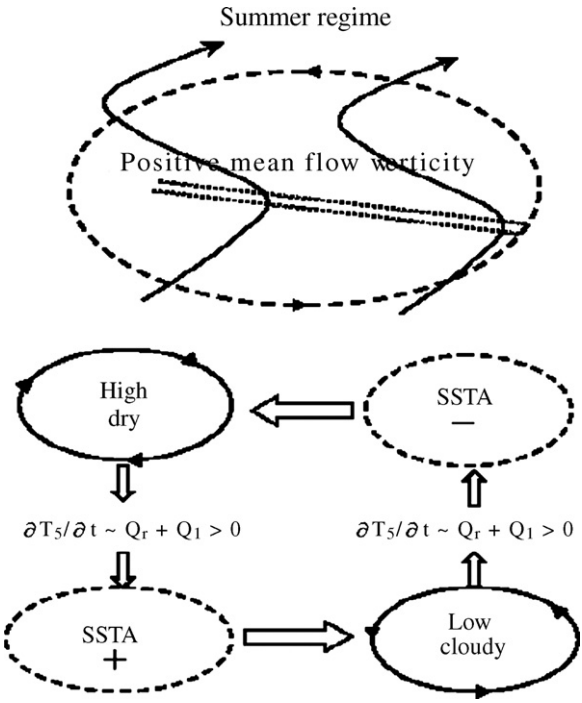

Fig. 7. Schematic diagram showing the air–sea feedback mechanism that sustains local intraseasonal oscillation over the SCS and the WNP. The nature of the air–sea interaction depends on the background circulation, which is shown on the top panel of the figure. The thin streamline with arrows denotes the seasonal mean flow and the double dashed line indicates the summer monsoon trough. The symbols, Q_r and Q_l denote, respectively, the downward short wave radiation flux and latent heat flux (adopted from Wang and Zhang, 2002).

maximum. The positive SST anomaly then increases convective instability, lowers surface pressure, and activates convection, thus turning the high-pressure (dry) anomaly to a low-pressure (wet) anomaly. Keeping this circular argument rolling, one finds that as long as the SCS and the WNP are controlled by a monsoon trough, air–sea interaction through both cloud-radiation and wind-evaporation/entrainment feedback processes would sustain ISO by providing a restoring mechanism. A theoretical analysis of the effects of this thermodynamic feedback on the coupled instability of the warm pool system (in the summer westerly regime) was previously offered by Wang and Xie (1998), who showed that the air–sea thermodynamic coupling may significantly amplify the off-equatorial moist Rossby modes and slow down their propagation.

5. Interannual variations

The SCS summer monsoon exhibits large year-to-year variations, which can be clearly seen from the time series of the SCSMI (Fig. 8a). The dominant spectrum peak seems different between the two reanalysis datasets; that is, a dominant 4–5-year period appears in NCEP–NCAR data (Fig. 8d) and two significant peaks are shown (3–4-year and 5–6-year periods) by ERA-40 data (Fig. 8c). This is mainly due to the different periods examined and the nonstationary nature of the SCS summer monsoon. The general 3–6-year periodicity tends to match that of ENSO.

5.1. Seasonal evolving interannual anomalies

The year-to-year variation of the SCS monsoon depends strongly on season. Wang and An (2005) have put forward a season-reliant empirical orthogonal function (S-EOF) analysis method to derive

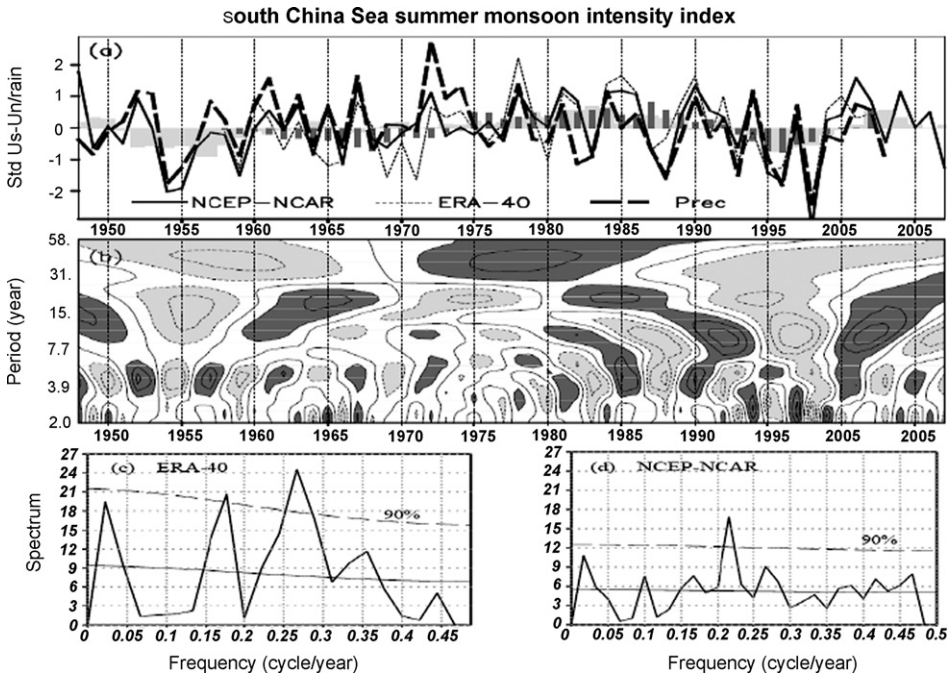

Fig. 8. (a) Time series of standardized SCS monsoon index (SCSMI) from 1948 to 2007. The solid and thin dashed lines are derived from the NCEP–NCAR reanalysis and ERA-40 data, respectively. The light grey and dark bars represent 7-year running means from the NCEP–NCAR reanalysis and ERA-40 data, respectively. The thick long-dashed line is standardized JJA land precipitation averaged over northern SCS (105°E–120°E, 10°N–20°N) derived from PREC/L rainfall data (Chen et al., 2002). (b) The corresponding real part distribution in frequency-time domain by morlet wavelet analysis of the SCSMI derived from the NCEP–NCAR reanalysis. (c) Spectrum analysis of the SCSMI derived from ERA-40 reanalysis (1958–2001). (d) Same as in (c) but for NCEP–NCAR reanalysis (1948–2007).

seasonally evolving anomalies throughout a full calendar year. In this study, we examined seasonal anomalies from the summer of Year 0, JJA(0), to spring of the following year (Year 1), MAM(1). Since the SCS monsoon involves active air–sea interaction, we used multivariate S-EOF analysis of precipitation, 850 hPa zonal and meridional winds, and SST. Such a multivariate method has the advantage of capturing spatial phase relationships among the various fields examined (e.g., Wang, 1992).

Fig. 9 shows spatial patterns and the principal component (PC) of the leading S-EOF mode obtained for the period of 1979–2006. The leading mode accounts for 33.1% of the total variance and is statistically distinguished from all other eigenvectors, according to the rule of North et al. (1982). In JJA(0), enhanced rainfall is seen over the central-northern SCS, which is associated with an anomalous cyclone at 850 hPa in the northern SCS and an enhanced westerly in the central SCS (Fig. 9a). During SON(0), the wet anomalies change drastically to dry anomalies associated with an anomalous anticyclone over the entire SCS (Fig. 9b). The dry anomalies then persist through the D(0)JF(1) and MAM(1) seasons (Fig. 9c and d). The PC time series (Fig. 9e) exhibits considerable interannual variations, which are closely related to ENSO, as evidenced by the high correlation coefficient (0.9) between PC1 and NIÑO 3.4 SSTA in D(0)JF(1). Therefore, the above seasonally evolving anomaly pattern concurs with ENSO turnabout. During the summer of El Niño development, the SCS summer monsoon is strong, but this strong monsoon turns into a persistent dry anomaly that lasts almost 1 year from the fall season marking El Niño development to the next summer (Fig. 9b–d; the figure for JJA(1) is not shown). This scenario is particularly true for the strong El Niño event. During La Niña, the anomalous condition over the SCS has a similar pattern but with opposite signs.

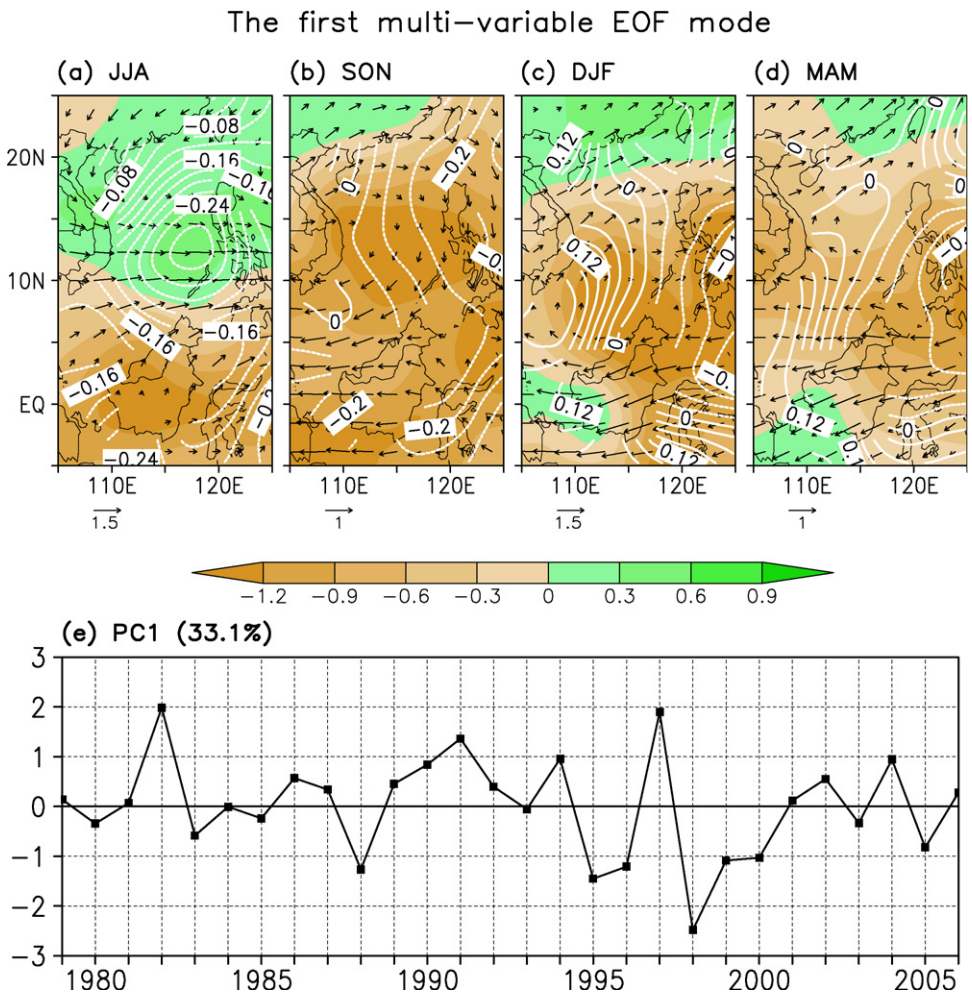

Fig. 9. Spatial pattern (a–d) and the corresponding principal components (e) of the anomalous seasonal mean 850 hPa winds (vectors), precipitation rate (color shading in mm/day), and SST (contours in °C) for the first multi-variable season-reliant EOF mode. The spatial patterns in (a–d) are for (a) JJA(0), (b) SON(0), (c) D(0)JF(1), and (d) MAM(1) season, respectively. The wind and SST data used are derived from NCEP/DOE reanalysis-2 and precipitation from CMAP.

The SCSMI, although designed for the boreal summer monsoon only, represents the leading principal component of the S-EOF reasonably well with a correlation coefficient of 0.68 for the period of 1979–2007 (Fig. 9e). This suggests that to a large extent, the SCSMI describes the seasonally evolving anomaly from year-to-year as well.

5.2. *Physical mechanisms behind the interannual variation of the SCS monsoon*

Fig. 9 indicates that ENSO is the dominant factor that controls the interannual variation of the SCS monsoon, but this is not a full story. In the El Niño's developing summer, the strong SCS summer monsoon is primarily due to the cyclonic anomaly associated with westerly anomalies in the equatorial western Pacific (Fig. 9a), which are a direct response to ENSO warming. From the summer to the ensuing fall, the cyclonic anomaly is suddenly replaced by an anomalous anticyclone (Fig. 9b). Wang and Zhang (2002) showed that the formation of the anomalous anticyclone is abrupt (within 1–2

weeks) and concurrent with a large swing from a wet to a dry phase of an ISO cycle, suggesting that atmospheric processes play an important role. Wang and Zhang (2002) attributed the establishment of the anomalous anticyclone to the early retreat of the EA summer monsoon (which results from the effect of remote El Niño forcing), extratropical–tropical interaction, and local air–sea interaction associated with ISO. (For details, please refer to that paper.)

From the fall to the next summer, a persistent drought over the SCS is caused by the quasi-stationary anomalous Philippine Sea anticyclone (PSAC). From winter to the subsequent summer, when remote El Niño forcing continues decaying, which mechanisms can maintain the PSAC anomaly and affect the SCS's climate? Wang et al. (2000) pointed out that the persistence of the PSAC cannot be accounted for by remote El Niño forcing alone. They attributed the PSAC's persistence to a positive thermodynamic feedback between the anomalous anticyclone and the underlying warm-pool ocean. In the presence of northeasterly trade winds (and the Asian winter monsoon), the increased total wind speed to the east of the PSAC's center induces excessive evaporation and entrainment cooling. The cooling to the east of the PSAC, in turn, suppresses convection and reduces latent heat release, which excites descending atmospheric Rossby waves that reinforce the PSAC in the course of their westward journey. This off-equatorial atmospheric Rossby wave-SST interaction theory has been confirmed by numerical experiments with the coupled GFDL AGCM-mixed-layer ocean model (Lau et al., 2004; Lau and Wang, 2006). The numerical experiments demonstrate that the interaction of the atmosphere and mixed-layer ocean can indeed amplify and sustain the anomalous PSAC, prolonging ENSO impact on the EA monsoon.

In addition to local atmospheric forcing, ocean dynamics also play a role in the SCS SST variability. The water exchange between the SCS and the Pacific through the Luzon Strait (LS) is of importance to the SCS (Wyrtki, 1961; Shaw, 1991; Qu, 2000; Fang et al., 2005). Qu et al. (2004) showed that the correlation coefficient between the LS transport and the Southern Oscillation index (SOI) is significant (0.63). The LS transport is stronger during El Niño years (e.g., 1982–1983, 1986–1987, and 1997–1998), and weaker during La Niña years (e.g., 1984–1985, 1988–1989, and 1996–1997).

6. Interdecadal variability

6.1. A sudden change around 1993 in the past 30 years

The interdecadal variability appears to be seasonally dependent. We found that the second S-EOF, as shown in Fig. 10, registers a sudden change around 1993, representing the major mode of interdecadal variation in the SCS monsoon in the past 30 years. Before 1993, a cyclonic circulation anomaly and enhanced convection prevailed in the SCS during JJA and SON; the anomalies sudden reverse their signs from SON to DJF. An anticyclonic circulation anomaly and suppressed convection then dominate the SCS during the following DJF and MAM seasons. After 1993, the JJA rainfall increases in southern China, the Indochina peninsula, and the northern SCS. This result supports the change detected by Kwon et al. (2005, 2007), who found that the EASM underwent a decadal change in the mid-1990s, and the relationship between the EA and the WNP summer monsoons experienced a significant decadal change around 1993/1994. Note also that after 1993, the SON rainfall drops in the southern SCS and the DJF and MAM rainfall increases in the central SCS. What causes this sudden interdecadal change remains unclear.

6.2. Strengthening of the SCSSM and ENSO relationship since the late 1970s

There is evidence indicating that interannual variability (IAV) of the SCS summer monsoon is not stationary. One such piece of evidence is seen from wavelet analysis of the SCS monsoon index, shown in Fig. 9b. The amplitude of the IAV has increased considerably since 1980. Before 1980, the oscillation period spans 4–5 years, and after 1980, it shifts to 7–10 years and quasi-biennially. The reason for this change may be due to interdecadal changes in ENSO forcing, because the interdecadal change of the SCSSM's IAV in frequency and amplitude is consistent with the increasing amplitude and periodicity change of ENSO events since the late 1970s. The latter has been well documented (Wang, 1995; Gu and Philander, 1995; An and Wang, 2000).

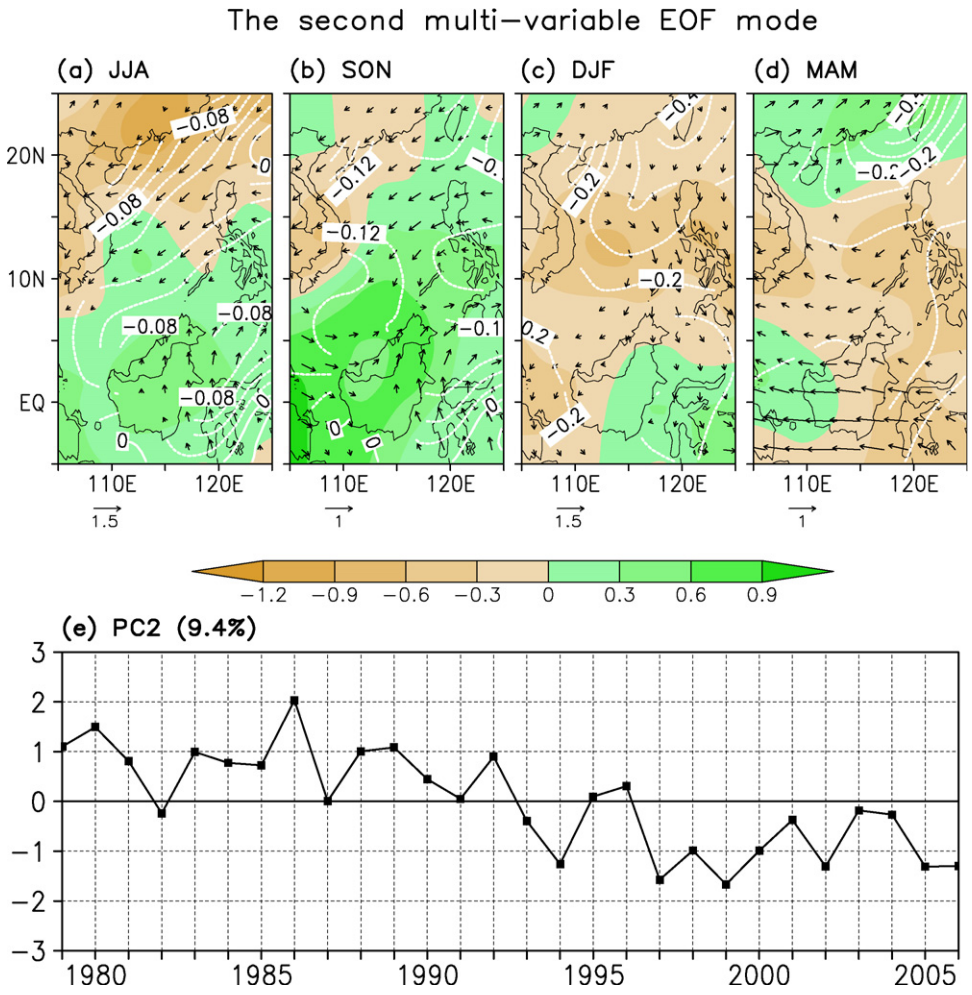

Fig. 10. The same as in Fig. 9 except for the second multi-variable S-EOF mode.

The interdecadal modulation of IAV also results from a strengthening relationship between the SCS monsoon and ENSO. In order to examine the relationship between SCSSM and ENSO, we show, in Fig. 11, the lead-lag correlation of the equatorial Indo-Pacific SST anomalies with reference to the JJA(0) SCSMI at various leads and lags for the period of (a) 1948–1977 and (b) 1978–2007, respectively. Evidently, the relationship between SCSSM and ENSO has experienced significant inter-decadal variation since the late 1970s. For the earlier epoch (1948–1977), the negative correlation between SCSSM and the eastern Pacific SST anomalies prior to the summer monsoon is weak, yet the correlation after the summer monsoon is strong (Fig. 11a). This result suggests that ENSO's impact on SCSSM is stronger in its development phase than in its decaying phase. On the other hand, for the period of 1978–2007, the increased negative correlation between the SCSSM and eastern Pacific SST anomalies in the previous winter implies that the SCSSM was strongly affected in the decaying phase of ENSO (Fig. 11b). The lead-lag correlation coefficients with Pacific SST are generally larger after the late 1970s, implying a strengthening relationship. This conclusion agrees with the results determined for the entire Asian-Australian monsoon system (Wang et al., 2008b).

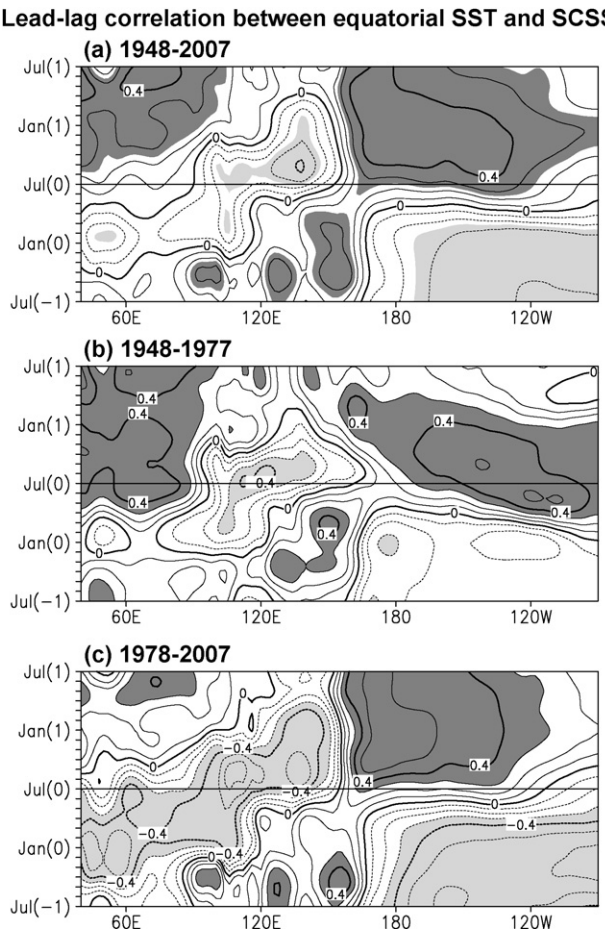

Fig. 11. The lead-lag correlation coefficients of the SST anomalies averaged between 5°S and 5°N with reference to the JJA SCSMI. The bold horizontal line indicates Jul (0) where the simultaneous correlations are shown. The dark shadings indicate statistical significant positive correlation exceeding 95% confidence level and light shadings are the counterpart for negative correlations.

6.3. Interdecadal modulation of the intraseasonal variability

The property of ISV is regulated by the annual cycle, and thus it is quite different between the early summer (May–July) and the late summer (August–October; Kemball-Cook and Wang, 2001; LinHo and Wang, 2002; Hsu et al., 2004; Kajikawa and Yasunari, 2005). The characteristics of the SCS ISV are also found to be modulated on the interannual timescale (Kajikawa and Yasunari, 2005) and on the interdecadal timescale (Zveryaev, 2002; Yang et al., 2008; Kajikawa et al., 2008).

Over the SCS, the intensity of the QBW and 30–50-day oscillations during June–July are anti-correlated on the interannual and interdecadal timescales. Yang et al. (2008) offered an explanation as follows. During the years of strong QBW oscillation, the June–July mean convection is enhanced over the equatorial western-central Pacific, and thus, the easterly vertical shear and low-level cyclonic meridional shear are enhanced over the western Pacific north of the equator. These conditions are favorable for active emanation of moist Rossby waves from the equatorial western Pacific, resulting in strong QBW over the SCS. On the other hand, the 30–50-day mode is closely related to the eastward propagation of MJO, and it becomes active when the large-scale background convection is enhanced

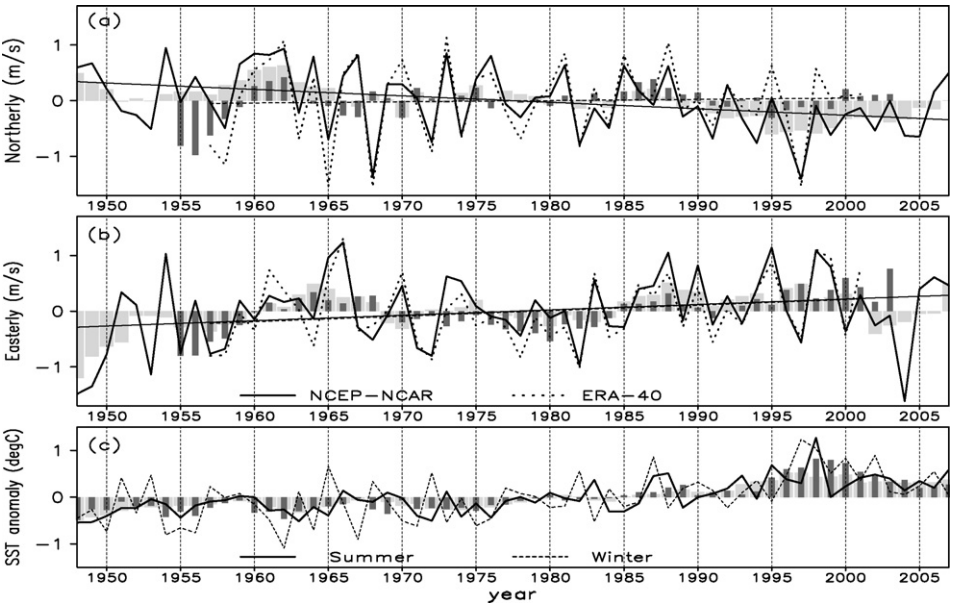

Fig. 12. Time series of DJF mean 850 hPa northerly (a) and easterly (b) wind speed anomaly averaged over (5°N–20°N, 110°E–120°E). The data used are from NCEP–NCAR (thick solid line) and ERA-40 (thick dotted line) reanalysis data. The thin solid (dashed) line is a linear trend obtained by least square fitting from NCEP–NCAR (ERA-40) data. The light grey (dark) bars represent a 5-year running mean time series for NCEP–NCAR (ERA-40) data. (c) Time series of JJA (solid line) and DJF (dashed line) SST anomaly and their 5-year running means (grey bar for JJA, dark bar for DJF) averaged over (5°N–20°N, 110°E–120°E).

over the eastern Indian Ocean and the Maritime Continent. One of these two large-scale settings often occurs in the absence of the other, so that when one mode is strong during the early summer, the other mode tends to be weak.

7. Long-term trends over the past 60 years

7.1. Strengthening trend of the SCS winter monsoon

Various indices have been used to quantify EA winter monsoon variability (e. g., Zhang et al., 1997; Jhun and Lee, 2004). These indices mainly reflect the activity of mid-latitude cold surges. The SCS is the southernmost part of the EA monsoon system, and as such, its variability is not only affected by the mid-latitude cold surge but also by changes in tropical convections. Climatologically, the maximum northeasterly wind speed in winter is located in the central SCS (Lu and Chan, 1999). Thus, the low-level northeasterly wind speed may be a good indicator of the strength of the SCS winter monsoon (Chang and Chen, 1992; Zhang et al., 1997).

Fig. 12a and b shows anomalous DJF mean northerly and easterly winds averaged over the SCS (5°N–20°N, 110°E–120°E). There is a significant descending trend in the northerly wind in the NCEP–NCAR reanalysis data, but no significant trend in the ERA40 reanalysis data (Fig. 12a). Therefore, the long-term trend in the meridional wind component over the SCS is inconclusive. However, the easterly wind component over the SCS shows a significant increasing trend in both of the reanalysis datasets (Fig. 12b). The northeasterly wind speed (figure not shown) has a similar increasing trend, and the correlation coefficient between the easterly component and the total wind speed is 0.97. This high correlation is due to the fact that the easterly wind component is much larger than the corresponding northerly component (Fig. 3d). Taken together, the result here suggests a strengthening trend in the SCS winter monsoon over the past 60 years.

7.2. Is there any trend in the SCS summer monsoon?

The intensity of the SCS summer monsoon has been measured differently in previous studies. These measures were primarily constructed by using either low-level winds or precipitation. All wind indices, which were defined by accumulated (or averaged) westerly, southwesterly, or southerly winds in the lower troposphere during the summer monsoon period, show a coherent decreasing trend from 1960 to 1998, suggesting a weakening SCSSM (Dai et al., 2000; Zhang et al., 2001; Liang et al., 2007). On the other hand, the indices constructed using precipitation or divergence show an increasing trend (Li and Long, 2001; Lin et al., 2004).

As shown in Section 3, the SCSMI is an excellent indicator of SCSSM rainfall and intensity. A positive (negative) index corresponds to abundant (deficient) rainfall over the central-northern SCS, and thus a strong summer monsoon (Fig. 4d). This simple objective index also allows for construction of a relatively long time series from 1948 to 2007.

The time series of the SCSSM's intensity or SCSMI during the past 60 years were computed by using 60-year NCEP–NCAR reanalysis data and 45-year (1958–2002) ERA40 reanalysis data (Fig. 8a). The indices derived from the two different datasets show consistent interannual and interdecadal variations. We note that no significant linear trend is found in the two datasets. This conclusion is supported by the 7-year running mean land-based rainfall averaged over (10°N–20°N, 105°E–120°E; Fig. 8a), and it is in general agreement with Kripalani and Kulkarni's assessment (1997) that there has been no systematic climate change or trend in any of the precipitation time series over the Southeast Asian domain.

Examination of lower boundary forcing (SST) indicates that the JJA mean SST anomaly averaged over the SCS appears to have a significant warming trend over the past 60 years and perhaps an interdecadal regime shift around the late 1970s (Fig. 12c). The interdecadal warming trend in the SCS SST agrees with the evolution of the dominant monsoon-ocean coupled mode over the SCS (Huang et al., 2007). It also agrees with the findings of Liang et al. (2007), who determined from *in situ* observation data that the SCS SST in summer has increased dramatically since 1978.

8. Challenging issues

It has been increasingly recognized that the SCS monsoon variability has large-scale implications for adjacent regions, including the WNP, EA, and the Maritime Continent. An improved seasonal prediction of the SCSSM may add predictability to prediction of the EA subtropical monsoon. Study of the SCS monsoon has received greater-than-ever attention since the SCS Monsoon Experiment in 1998. Remarkable progress has been made in the last decade in studying climate variations of the SCS monsoon. The present review can only take into account some of the important progress made. Many scientific issues remain outstanding.

The abrupt, simultaneous onset of the SCSSM over a large latitude range (about 20°) is unique. The SCSSM onset has been considered a precursor to East Asian summer monsoon development (Tao and Chen, 1987; Lau and Yang, 1997). In contrast to the relatively "punctual" onset of the Indian summer monsoon at Kerala, the onset of the SCSSM exhibits considerable year-to-year variations. What controls the year-to-year variability of the SCSSM onset date? To what extent is the summer monsoon onset predictable? These questions remain controversial, and the underlying physics is not well understood. A major roadblock in the study of onset variability is the lack of a generally recognized definition of onset dates. The current definitions of the onset dates are extremely diverse (e.g., He et al., 2001; Wang et al., 2004), and no progress can be made if this problem is not resolved.

The QBW is a prominent component of ISV over the SCS. But the mechanisms that sustain QBW oscillation remain unrivaled. The practical predictability of the QBW and 30–50-day modes has not been assessed with the dynamical prediction models. Also needed is to determine to what extent the interannual variations of the two intraseasonal modes are predictable.

On an interannual timescale, while we know ENSO is the major source of predictability for SCS monsoon variations, we do not thoroughly know about other influential factors. Identification of these factors is important for seasonal prediction, especially during ENSO-neutral years.

On an interdecadal timescale, the 1993/1994 decadal change during the last three decades seems to be a robust signal and may be related to decadal changes in the WNP typhoon track (Kwon et al., 2007) and variation in the WNP subtropical high (Sui et al., 2007). However, the specific factors that are important in accounting for this interdecadal shift remain to be explained.

The trend of a strengthening winter monsoon in the past 60 years is expected to induce an increasing trend in the precipitation along the windward (east) side of the mountains on the eastern coasts of the Philippines, Vietnam, and Malaysia. But no such trends have been reported to the authors' knowledge. Further, as total wind speed increases, the ocean's latent heat loss would increase, but the DJF mean SST averaged over the SCS shows an upward trend (Fig. 12c). There must be other factors, such as increasing solar forcing, that overcome the evaporation/entrainment cooling due to the increased wind speed. A detailed budget analysis is needed to pin down the exact causes of the SCS warming trend.

What causes the increasing trend of the winter monsoon is another issue that needs to be addressed. Since the SST is rising, it is unlikely that the mid-latitude cold surge plays a major role in the enhancement of the wind speed. Peng et al. (2003) proposed that the trend of the enhancing winter monsoon may be constrained by the changes in the thermal contrast between the land and the adjacent sea, perhaps due to global warming. However, while the SCS SST has an increasing trend, the land surface temperature in mid-latitude has increased more, so it is not clear whether the temperature difference between the SCS and its adjoining land region has increased in the past. We speculate that the strengthening of the SCS winter easterly is a response to changes in tropical precipitation (latent heating). Further research is required to test this hypothesis.

Acknowledgements

This research is supported by NSF Climate Dynamics Program (Grant ATM-0647995) and by the Japan Agency for Marine-Earth Science and Technology (JAMSTEC), NASA, and NOAA through their sponsorship of the IPRC. Fei Huang and Zhiwei Wu acknowledge the support of the National Natural Science Foundation of China (Grant Nos. 40775042 and 40605022) and the National Basic Research Program "973" (Grant No. 2006CB403600). Jing Yang acknowledges the funding from the CAS International Partnership Project and the 973 Project (Grant 2006CB403602). This paper is SOEST contribution number 7571 and IPRC contribution number 554.

References

An, S.-I., Wang, B., 2000. Interdecadal change of the structure of ENSO mode and its impact on the ENSO frequency. J. Climate 13, 2044–2055.

Annamalai, H., Slingo, J.M., 2001. Active/break cycles: diagnosis of the intraseasonal variability of the Asian summer monsoon. Climate Dyn. 18, 85–102.

Chan, J.C.L., Ai, W.X., Xu, J.J., 2002. Mechanisms responsible for the maintenance of the 1998 South China Sea summer monsoon. J. Meteorol. Soc. Jpn. 80, 1103–1113.

Chang, C.-P., Chen, J.M., 1992. A statistical study of winter monsoon cold surges over the South China Sea and the large-scale equatorial divergence. J. Meteorol. Soc. Jpn. 70, 287–302.

Chang, C.-P., Wang, Z., McBride, J., Liu, C.H., 2005a. Annual cycle of Southeast Asia—Maritime Continent rainfall and the asymmetric monsoon transition. J. Climate 18, 287–301.

Chang, C.-P., Harr, P.A., Chen, H.J., 2005b. Synoptic disturbances over the equatorial South China Sea and western Maritime Continent during boreal winter. Mon. Weather Rev. 133, 489–503.

Chang, C.-P., Wang, Z., Hendon, H., 2006. The Asian Winter monsoon. In: Wang, B. (Ed.), The Asian Monsoon. Praxis, Berlin, pp. 89–127.

Chatterjee, P., Goswami, B.N., 2004. Structure, genesis and scale selection of the tropical quasi-biweekly mode. Quart. J. R. Meteorol. Soc. 130, 1171–1194.

Chen, T., Chen, J., 1993. The 10–20-day mode of the 1979 Indian monsoon: its relation with the time variation of monsoon rainfall. Mon. Weather Rev. 121, 2465–2482.

Chen, T.-C., Chen, J.R., 1995. An observational study of the South China Sea monsoon during the 1979 summer—onset and life-cycle. Mon. Weather Rev. 123, 2295–2318.

Chen, T.-C., Murakami, M., 1988. The 30–50 day variation of convective activity over the Western Pacific-Ocean with Emphasis on the Northwestern Region. Mon. Weather Rev. 116, 892–906.

Chen, M., Xie, P., Janowiak, J.E., Arkin, P.A., 2002. Global land precipitation: a 50-yr monthly analysis based on Gauge observations. J. Hydrometeor. 3, 249–266.

Chen, T.-C., Yoon, J., 2000. Interannual variation in Indochina summer monsoon rainfall: possible mechanism. J. Climate 13, 1979–1986.

Dai, N.J., Xie, A., Zhang, Y., 2000. Interannual and interdecadal variations of summer monsoon activities over South China Sea. Climatic Environ. Res. 5, 363–374 (in Chinese).
Ding, Y.-H., 1992. Summer monsoon rainfall in China. J. Meteorol. Soc. Jpn. 70, 373–396.
Ding, Y.-H, Li, C.Y., Li, Y.J., 2004. Overview of the South China Sea monsoon experiment (SCSMEX). Adv. Atmos. Sci. 21, 1–18.
Drbohlav, H.-K.L., Wang, B., 2005. Mechanism of the northward propagating intraseasonal oscillation in the south Asian monsoon region: insights from a zonally averaged model. J. Climate 18, 952–972.
Fang, G., Susanto, R.D., Soesilo, I., Zheng, Q., Qiao, F., Wei, Z., 2005. A note on the South China Sea shallow interocean circulation. Adv. Atmos. Sci. 22, 946–954.
Ferranti, L., Slingo, J., Palmer, T., Hoskins, B., 1997. Relations between interannual and intraseasonal monsoon variability diagnosed from AMIP integrations. Quart. J. R. Meteorol. Soc. 123, 1323–1357.
Fu, X., Wang, B., 2004. Differences of boreal summer intraseasonal oscillations simulated in an atmosphere–ocean coupled model and an atmosphere-only model. J. Climate 17, 1263–1271.
Fu, X., Wang, B., Li, T., McCreary, J., 2003. Coupling between northward-propagating. intraseasonal oscillations and sea surface temperature in the Indian Ocean. J. Atmos. Sci. 60, 1733–1753.
Fukutomi, Y., Yasunari, T., 1999. 10–25-day intraseasonal variations of convection and circulation over East Asia and western North Pacific during early summer. J. Meteorol. Soc. Jpn. 77, 753–769.
Fukutomi, Y., Yasunari, T., 2002. Tropical–extratropical interaction associated with the 10–25-day oscillation over the western Pacific during the Northern summer. J. Meteorol. Soc. Jpn. 80, 311–331.
Goswami, P., Mathew, V., 1994. A mechanism of scale selection in tropical circulation at observed intraseasonal frequencies. J. Atmos. Sci. 51, 3155–3166.
Gill, A., 1980. Some simple solutions for heat-induced tropical circulation. Quart. J. R. Meteorol. Soc. 106, 447–462.
Gu, D., Philander, S.G.H., 1995. Secular changes of annual and interannual variability in the tropics during the past century. J. Climate 8, 864–876.
He, J., Ding, Y., Gao, H., Xu, H., 2001. The Definition of Onset Date of South China Sea Summer Monsoon and the Monsoon Indices. China Meteorological Press, Beijing, 123 pp. (in Chinese).
Hsu, H.-H., Weng, C.H., 2001. Northwestward propagation of the intraseasonal oscillation in the western North Pacific during the boreal summer: structure and mechanism. J. Climate 14, 3834–3850.
Hsu, H.-H., Weng, C.-H., Wu, C.-H., 2004. Contrasting characteristics between the northward and eastward propagation of the intraseasonal oscillation during the boreal summer. J. Climate 17, 727–743.
Huang, F., Wang, H., Dai, P., 2007. Spatial-temporal characters of the monsoon-ocean coupled mode over the South China Sea and its relation with summer precipitation of China. Periodical Ocean Univ. China 37, 351–356.
Hung, C., Yanai, M., 2004. Factors contributing to the onset of the Australian summer monsoon. Quart. J. R. Meteorol. Soc. 130, 739–761.
Jhun, J.G., Lee, E.J., 2004. A new East Asian winter monsoon index and associated characteristics of the winter monsoon. J. Climate 17, 711–726.
Jiang, X.N., Li, T., Wang, B., 2004. Structures and mechanisms of the northward propagating boreal summer intraseasonal oscillation. J. Climate 17, 1022–1039.
Kajikawa, Y., Yasunari, T., 2005. Interannual variability of the 10–25- and 30–60-day variation over the South China Sea during boreal summer. Geophys. Res. Lett. 32, L04710, doi:10.1029/2004GL021836.
Kajikawa, Y., Yasunari, T., Wang, B., 2008. Two types of low-frequency intraseasonal oscillation over the South China Sea. Geophys. Res. Lett.
Kanamitsu, M., Ebisuzaki, W., Woollen, J., Yang, S.K., Hnilo, J.J., Fiorino, M., Potter, G.L., 2002. NCEP–DOE AMIP-II reanalysis (R-2). Bull. Am. Meteorol. Soc. 83, 1631–1643.
Kang, I., An, S., Ho, C., Lim, Y., Lau, K., 1999. Principal modes of climatological seasonal and intraseasonal variations of the Asian summer monsoon. Mon. Weather Rev. 127, 322–340.
Kawamura, R., Murakami, T., Wang, B., 1996. Tropical and mid-latitude 45-day perturbations over the Western Pacific during the northern summer. J. Meteorol. Soc. Jpn. 74, 867–890.
Kemball-Cook, S., Wang, B., 2001. Equatorial waves and air–sea interaction in the boreal summer intraseasonal oscillation. J. Climate 14, 2923–2942.
Kripalani, R.H., Kulkarni, A., 1997. Rainfall variability over South-east Asia–connections with Indian monsoon and enso extremes: new perspectives. Int. J. Climatol. 17, 1155–1168.
Krishnamurti, T., Bhalme, H., 1976. Oscillations of a monsoon system. Part I. Observational aspects. J. Atmos. Sci. 33, 1937–1954.
Krishnamurti, T.N., Ardanuy, P., 1980. The 10 to 20 day westward propagating modes and 'breaks in the monsoons'. Tellus 32, 15–26.
Kwon, M., Jhun, J.-G., Wang, B., An, S.-I., Kug, J.-S., 2005. Decadal change in relationship between East Asian and WNP summer monsoons. Geophys. Res. Lett. 32, L16709, doi:10.1029/2005GL023026.
Kwon, M., Jhun, J.-G., Ha, K.-J., 2007. Decadal change in East Asian summer monsoon circulation in the mid-1990s. Geophys. Res. Lett. 34, L21706, doi:10.1029/2007GL031977.
Lau, K.M., 1995. The South China Sea monsoon experiment (SCSMEX): Science Plan. 61 pp.
Lau, K.M., et al., 2000. A report of field operations and early results of the South China Sea monsoon experiment (SCSMEX). Bull. Am. Meteorol. Soc. 81, 1261–1270.
Lau, K.M., Chan, P.H., 1986. Aspects of the 40–50 day oscillation during the northern summer as inferred from outgoing longwave radiation. Mon. Weather Rev. 114, 1354–1367.
Lau, K.-M., Chang, F., 1992. Tropical intraseasonal oscillation and its prediction by the NMC operation model. J. Climate, 1365–1378.
Lau, K.-M., Yang, S., 1997. Climatology and interannual variability of the Southeast Asian summer monsoon. Adv. Atmos. Sci. 14, 141–162.
Lau, N.-C., Nath, M.J., Wang, H., 2004. Simulations by a GFDL GCM of ENSO-related variability of the coupled atmosphere–ocean system in the East Asian monsoon region. *East Asian Monsoon*. World Scientific Publishing Company Book Series, 2.
Lau, N.-C., Wang, B., 2006. Chapter 12: Interactions between the Asian monsoon and the El Niño-Southern Oscillation. In: Wang, B. (Ed.), The Asian Monsoon. Springer-Verlag, New York.

Lawrence, D.M., Webster, P.J., 2002. The boreal summer intraseasonal oscillation: relationship between northward and eastward movement of convection. J. Atmos. Sci. 59, 1593–1606.
Li, C.Y., Long, Z.X., 2001. A South China Sea summer monsoon onset index and its interannual variability. In: He, J.H., Ding, Y.H., Gao, H. (Eds.), Dates of Summer Monsoon Onset in the South China Sea and Monsoon Indices. China Meteorological Press, Beijing, pp. 78–82 (in Chinese).
Liang, J.Y., Yang, S., Li, C., Li, X., 2007. Long-term changes in the South China Sea summer monsoon revealed by station observations of the Xisha Islands. J. Geophys. Res. 112, D10104, doi:10.1029/2006JD007922.
Lin, A.L., Liang, J.Y., Gu, D.J., Wang, D.X., 2004. On the relationship between convection intensity of South China Sea summer monsoon and air–sea temperature difference in the tropical oceans. Acta Oceanol. Sin. 23, 267–278.
LinHo, Wang, B., 2002. The time-space structure of the Asian-Pacific summer monsoon: a fast annual cycle view. J. Climate 15, 2001–2019.
Liu, J., Wang, B., Yang, J., 2008. Forced and internal modes of the east asiam monsoon. Climate in the Past Discussion, Revised.
Liu, Q., Yang, H., Wang, Q., 2000. Dynamic characteristics of seasonal thermocline in the deep sea region of the South China Sea. J. Oceanol. Limnol. 18, 104–109 (in Chinese).
Liu, Q., Jiang, X., Xie, S.-P., Liu, W.T., 2004. A gap in the Indo-Pacific warm pool over the South China Sea in boreal winter: seasonal development and interannual variability. J. Geophys. Res. 109, C07012, doi:10.1029/2003JC002179.
Lu, E., Chan, J., 1999. A unified monsoon index for South China. J. Climate 12, 2375–2385.
Madden, R.A., Julian, P.R., 1971. Detection of a 40–50 day oscillation in the zonal wind in the tropical Pacific. J. Atmos. Sci. 29, 1109–1123.
Madden, R.A., Julian, P.R., 1972. Description of large-scale circulations cells in the tropics with a 40–50 day period. J. Atmos. Sci. 28, 702–708.
Madden, R.A., Julian, P.R., 1994. Observations of the 40–50 day tropical oscillation—a review. Mon. Weather Rev. 122, 814–837.
Mao, J.Y., Chan, J.C.L., 2005. Intraseasonal variability of the South China Sea summer monsoon. J. Climate 18, 2388–2402.
Matsumoto, J., Murakami, T., 2002. Seasonal migration of monsoons between the northern and southern hemisphere as revealed from equatorially symmetric and asymmetric OLR data. J. Meteorol. Soc. Jpn. 80, 419–437.
Meehl, G., 1987. The annual cycle and interannual variability in the tropical Pacific and Indian Ocean region. Mon. Weather Rev. 115, 27–50.
Murakami, T., 1976. Analysis of summer monsoon fluctuations over India. J. Meteorol. Soc. Jpn. 54, 15–31.
Murakami, T., 1980. Empirical orthogonal function analysis of satellite observed out-going longwave radiation during summer. Mon. Weather Rev. 108, 205–222.
Murakami, T., Matsumoto, J., 1994. Summer monsoon over the Asian continent and western north Pacific. J. Meteorol. Soc. Jpn. 72, 719–745.
Nakazawa, T., 1992. Seasonal phase lock of intraseasonal variation during the Asian summer monsoon. J. Meteorol. Soc. Jpn. 70, 257–273.
Nitta, T., 1987. Convective activities in the tropical western Pacific and their impact on the northern-hemisphere summer circulation. J. Meteorol. Soc. Jpn. 65, 373–390.
North, G.R., Bell, T.L., Cahalan, R.F., Moeng, F.J., 1982. Sampling errors in the estimation of empirical orthogonal functions. Mon. Weather Rev. 110, 699–706.
Peng, Z.C., Chen, T.G., Nie, B.F., Head, M.J., He, X.X., Zhou, W.J., 2003. Coral delta O-18 records as an indicator of winter monsoon intensity in the South China Sea. Quart. Res. 59, 285–292.
Qu, T., 2000. Upper layer circulation in the South China Sea. J. Phys. Oceanogr. 30, 1450–1460.
Qu, T., Kim, Y.Y., Yaremchuk, M., Tozuka, T., Ishida, A., Yamagata, T., 2004. Can Luzon Strait transport play a role in conveying the impact of ENSO to the South China Sea? J. Climate 17, 3644–3657.
Shaw, P.-T., 1991. The seasonal variation of the intrusion of the Philippines Sea water into the South China Sea. J. Geophys. Res. 96, 821–827.
Sui, C.-H., Chung, P.-H., Li, T., 2007. Interannual and interdecadal variability of the summertime western North Pacific subtropical high. Geophys. Res. Lett. 34, L11701, doi:10.1029/2006GL029204.
Tanaka, M., 1992. Intraseasonal oscillation and the onset and retreat dates of the summer monsoon over East. Southeast Asia and the western Pacific region using GMS high cloud amount data. J. Meteorol. Soc. Jpn. 70, 613–629.
Tao, S., Chen, L.-X., 1987. A review of recent research on the East Asian summer monsoon in China. In: Chang, C.-P., Krishnamurti, T.N. (Eds.), Monsoon Meteorology. Oxford University Press, New York, pp. 60–92.
Waliser, D., Weickmann, K., Dole, R., Schubert, S., Alves, O., et al., 2006. The experimental MJO prediction project. Bull. Am. Meteorol. Soc. 87, 425–431.
Wang, B., 1992. The vertical structure and development of the ENSO anomaly mode during 1979–1989. J. Atmos. Sci. 49, 698–712.
Wang, B., 1994. Climatic regimes of tropical convection and rainfall. J. Climate 7, 1109–1118.
Wang, B., 1995. Interdecadal changes in El Niño onset in the last four decades. J. Climate 8, 267–285.
Wang, B., 2005. Theories. In: Lau, K.-M., Waliser, D.E. (Eds.), Intraseasonal Variability of the Atmosphere-Ocean Climate System. Springer-Verlag, Heidelberg, Germany.
Wang, B., An, S.-I., 2005. A method for detecting season-dependent modes of climate variability: S-EOF analysis. Geophys. Res. Lett. 32, L15710.
Wang, B., Ding, Q., 2008. The global monsoon: major modes of annual variations in the tropics. Dyn. Atmos. Ocean 44, 165–183.
Wang, B., Fan, Z., 1999. Choice of South Asian summer monsoon indices. Bull. Am. Meteorol. Soc. 80, 629–638.
Wang, B., LinHo, 2002. Rainy seasons of the Asian-Pacific monsoon. J. Climate 15, 386–398.
Wang, B., Rui, H., 1990. Synoptic climatology of transient tropical intraseasonal convection anomalies—1975–1985. Meteorol. Atmos. Phys. 44, 43–61.
Wang, B., Wu, R., 1997. Peculiar temporal structure of the South China Sea summer monsoon. Adv. Atmos. Sci. 14, 177–194.
Wang, B., Xie, X., 1997. A model for the boreal summer intraseasonal oscillation. J. Atmos. Sci. 54, 72–86.
Wang, B., Xie, X., 1998. Coupled modes of the warm pool climate system. Part I. The role of air–sea interaction in maintaining Madden–Julian Oscillation. J. Climate 11, 2116–2135.

Wang, B., Xu, X., 1997. Northern hemisphere summer monsoon singularities and climatological intraseasonal oscillation. J. Climate 10, 1071–1085.
Wang, B., Zhang, Q., 2002. Pacific-East Asian teleconnection. Part II. How the Philippine Sea anticyclone established during development of El Niño. J. Climate 15, 3252–3265.
Wang, B., Lin, H., Zhang, Y.S., Lu, M.-M., 2004. Definition of South China Sea monsoon onset and commencement of the East Asia summer monsoon. J. Climate 17, 699–710.
Wang, B., Wu, R., Fu, X., 2000. Pacific–East Asian teleconnection: how does ENSO affect East Asian climate? J. Climate 13, 1517–1536.
Wang, B., Webster, P., Kikuchi, K., Yasunari, T., Qi, Y., 2006. Boreal summer quasi-monthly oscillation in the global tropics. Climate Dyn. 27, 661–675.
Wang, B., Wu, Z., Li, J., Liu, J., Chang, C.-P., Ding, Y., Wu, G., 2008a. How to measure the strength of the East Asian summer monsoon? J. Climate 21, 4449–4463.
Wang, B., Yang, J., Zhou, T.J., Wang, B., 2008b. Interdecadal changes in the major modes of Asian–Australian monsoon variability: strengthening relationship with ENSO since the late 1970s. J. Climate 21, 1771–1789.
Wang, P., 1999. Response of Western Pacific marginal seas to glacial cycles: paleoceanographic and sedimentological features. Mar. Geol. 156, 5–40.
Wyrtki, K., 1961. Physical oceanography of the southeast Asian waters. Naga Rep. 2, Scripps Inst. of Oceanogr., La Jolla, Calif., 195.
Xie, P., Arkin, P.A., 1997. Global precipitation: a 17-year monthly analysis based on gauge observations, satellite estimates and numerical model outputs. Bull. Am. Meteorol. Soc. 78, 2539–2558.
Yang, J., Wang, B., Wang, B., 2008. Anticorrelated intensity change of the quasi-biweekly and 30–50 day oscillations over the South China Sea. Geophys. Res. Lett. 35, L16702, doi:10.1029/2008GL034449.
Yasunari, T., 1991. The monsoon year: a new concept of the climate year in the tropics. Bull. Am. Meteorol. Soc. 72, 1331–1338.
Zhang, X.Z., Li, J.L., Yan, J.Y., Ding, Y.H., 2001. A study of circulation characteristics and index of the South China Sea summer monsoon. In: He, J.H., Ding, Y.H., Gao, H. (Eds.), Dates of Summer Monsoon Onset in the South China Sea and Monsoon Indices. China Meteorological Press, Beijing, pp. 83–95 (in Chinese).
Zhang, Y., Sperber, K., Boyle, J., 1997. Climatology and interannual variation of the East Asian winter monsoon: results from the 1979–95 NCEP/NCAR reanalysis. Mon. Weather Rev. 125, 2605–2619.
Zhu, C.W., Nakazawa, T., Li, J.P., 2003. The 30–60 day intraseasonal oscillation over the western North Pacific Ocean and its impacts on summer flooding in China during 1998. Geophys. Res. Lett. 30, 1952, doi:10.1029/2003GL017817.
Zhu, Q.G., He, J.H., Wang, P.X., 1986. A study of circulation differences between East-Asian and Indian summer monsoons with their interactions. Adv. Atmos. Sci. 3, 466–477.
Zveryaev, I.I., 2002. Interdecadal changes in the zonal wind and the intensity of intraseasonal oscillations during boreal summer Asian monsoon. Tellus Ser. A: Dyn. Meteorol. Oceanol. 54, 288–298.